AMERICAN SOCIETY FOR MICROBIOLOGY | Journal of Bacteriology®

RESEARCH ARTICLE

Bacillus subtilis Regulators MntR and Zur Participate in Redox Cycling, Antibiotic Sensitivity, and Cell Wall Plasticity

Paola Randazzo,[a*] Jamila Anba-Mondoloni,[a] Anne Aubert-Frambourg,[a] Alain Guillot,[a] Christine Pechoux,[b] Jasmina Vidic,[a] Sandrine Auger[a]

[a]Micalis Institute, INRA, AgroParisTech, Université Paris-Saclay, Jouy-en-Josas, France

[b]Génétique Animale et Biologie Intégrative, Université Paris-Saclay, UMR1313, INRA, Jouy-en-Josas, France

ABSTRACT The *Bacillus subtilis* MntR and Zur transcriptional regulators control homeostasis of manganese and zinc, two essential elements required in various cellular processes. In this work, we describe the global impact of *mntR* and *zur* deletions at the protein level. Using a comprehensive proteomic approach, we showed that 33 and 55 proteins are differentially abundant in Δ*mntR* and Δ*zur* cells, respectively, including proteins involved in metal acquisition, translation, central metabolism, and cell wall homeostasis. In addition, both mutants showed modifications in intracellular metal ion pools, with significant Mg^{2+} accumulation in the Δ*mntR* mutant. Phenotypic and morphological analyses of Δ*mntR* and Δ*zur* mutants revealed their high sensitivity to lysozyme, beta-lactam antibiotics, and external oxidative stress. Mutant strains had a modified cell wall thickness and accumulated lower levels of intracellular reactive oxygen species (ROS) than the wild-type strain. Remarkably, our results highlight an intimate connection between MntR, Zur, antibiotic sensitivity, and cell wall structure.

IMPORTANCE Manganese and zinc are essential transition metals involved in many fundamental cellular processes, including protection against external oxidative stress. In *Bacillus subtilis*, Zur and MntR are key transcriptional regulators of zinc and manganese homeostasis, respectively. In this work, proteome analysis of *B. subtilis* wild-type, Δ*mntR*, and Δ*zur* strains provided new insights into bacterial adaptation to deregulation of essential metal ions. Deletions of *mntR* and *zur* genes increased bacterial sensitivity to lysozyme, beta-lactam antibiotics, and external oxidative stress and impacted the cell wall thickness. Overall, these findings highlight that Zur and MntR regulatory networks are connected to antibiotic sensitivity and cell wall plasticity.

KEYWORDS *Bacillus*, metal, MntR, proteomics, Zur, stress

Metal ions such as iron, zinc, and manganese are crucial for central cellular processes, as they are structural components of many proteins and membranes while participating in the catalysis of metabolic reactions and electron transfer. However, metals are highly toxic when in excess. The mammalian innate immune system responds to infection by combining deprivation of some metals (Fe, Zn, and Mn) with a metal poisoning strategy (Cu and Zn) to prevent bacterial replication (1–3). Restrictive access to critical transition metals is a defense known as nutritional immunity (4). Examples involve lipocalin, which binds siderophores and thereby prevents Fe acquisition by bacterial pathogens (5), and calprotectin, which restricts acquisition of Zn or Mn (6). In the macrophage phagosome, NRAMP1 removes Mn and Fe to starve intracellular pathogens (7, 8). In contrast, in macrophage antimicrobial pathways, Zn and Cu toxicity is used to combat invading microbes.

Among transition metals, Mn and Zn are important in many fundamental cellular

Citation Randazzo P, Anba-Mondoloni J, Aubert-Frambourg A, Guillot A, Pechoux C, Vidic J, Auger S. 2020. *Bacillus subtilis* regulators MntR and Zur participate in redox cycling, antibiotic sensitivity, and cell wall plasticity. J Bacteriol 202:e00547-19. https://doi.org/10.1128/JB.00547-19.

Editor Tina M. Henkin, Ohio State University

Address correspondence to Jasmina Vidic, jasmina.vidic@inra.fr, or Sandrine Auger, sandrine.auger@inra.fr.

* Present address: Paola Randazzo, Department of Biotechnology, Delft University of Technology, Delft, The Netherlands.

Received 27 August 2019
Accepted 26 November 2019
Accepted manuscript posted online 9 December 2019
Published 11 February 2020

TABLE 1 *B. subtilis* strains used in this study

Strain	Genotype[a]	Reference or source
BSB1	*trp*$^+$	76
BSAS45	Δ*zur*::*aphA3*	31
BSAS46	Δ*mntR*::*aphA3*	This work

[a]*aphA3*, *Enterococcus faecalis* kanamycin resistance gene.

processes, including protection against reactive oxygen species (ROS). There is now evidence that the invading microbe utilizes Mn as a key micronutrient to counteract the effects of host-mediated oxidative stress. Thus, Mn plays a significant role in adaptation of pathogenic bacteria to the human host (9). It protects bacterial cells from oxidative stress, either as a cofactor for Mn-dependent catalases and superoxide dismutases or via its inherent ability to quench free-radical-mediated reactions (9–11). Similarly, Zn is important for resistance to both hydrogen peroxide (H_2O_2) and the thiol-oxidizing agent diamide (12). Zn^{2+} may protect thiols from oxidation and even displace other redox-active metals in protein thiol-containing active sites to maintain the function of proteins (13). Pathogenic bacteria deficient in maintaining proper metal homeostasis are less virulent (2, 8, 14, 15).

Intracellular metal homeostasis in bacteria is ensured by finely tuned import and efflux systems (16). Metalloregulatory proteins act as metal-sensing regulatory transcription factors. In the Gram-positive bacterium *Bacillus subtilis*, MntR and Zur are key regulators of manganese and zinc homeostasis, respectively. MntR is a bifunctional regulator that binds Mn^{2+} as an effector (17, 18). The MntR regulon includes 7 genes involved in Mn^{2+} uptake or efflux (18–22). The Zur metalloprotein binds Zn^{2+} as a corepressor (23–26). The Zur regulon contains 11 genes, including genes for zinc transporters (12, 23) and zinc-independent alternative ribosomal proteins (27–30). However, Zur binds 80 regions on the chromosome, indicating far broader control by this regulator (31). Zinc homeostasis is also maintained via a zinc-inducible efflux pump, CzcD, which is regulated at the transcriptional level by the metalloregulator CzrA (22). Together, Zur and CzrA sense changes in the labile Zn^{2+} pool and modify expression of genes encoding proteins that mediate zinc homeostasis (32, 33).

The roles of the MntR and Zur proteins at the transcriptional level have been studied extensively. However, a study of the global impact of *mntR* and *zur* deletions at the protein level is still missing. Here, we performed a comprehensive study on global protein changes in *B. subtilis* Δ*mntR* and Δ*zur* mutants by quantitative proteomic analysis and validated the obtained results by physiology tests and microscopy observation. Together, our results show that Zur and MntR regulators are necessary to ensure bacterial fitness upon environmental stress.

RESULTS

Impact of *mntR* and *zur* deletions on the *B. subtilis* proteome. To understand the physiological state of cells with the deleted *mntR* or *zur* gene deleted, we performed a comparative analysis of the cytosolic and membrane proteome of Δ*mntR*, Δ*zur*, and wild-type (WT) cells grown in exponential phase (Table 1). Optimized analyses by liquid chromatography-tandem mass spectrometry (LC-MS/MS) of four technical replicates resolved more than 1,700 proteins (see Table S1 in the supplemental material). In total, 33 and 55 proteins were statistically significantly differentially abundant ($P < 0.05$ by the Kruskal-Wallis test and one-way analysis of variance [ANOVA]) in Δ*mntR* and Δ*zur* cells, respectively (Table 2). Twelve proteins were common between Δ*mntR* and Δ*zur* proteomic data sets (Fig. 1A). Among them, CarB and Spo0M changes in regulation diverged between the two mutants. Proteins involved in metal acquisition, translation, stress response, cell wall synthesis, and amino acid/nitrogen/carbon metabolism were mainly affected in Δ*mntR* and Δ*zur* mutants (Fig. 1B and C).

The proteome analysis of the Δ*mntR* mutant indicated a greater increase of the MntA and MntB proteins, as expected since they are components of the MntABCD Mn uptake systems (Table 3). Of note, proteins of the Mn^{2+} efflux systems, MneP and MneS,

TABLE 2 Total proteins differentially abundant in the cytosolic and membrane fractions of the *B. subtilis* Δ*mntR* and Δ*zur* mutants

	No. of proteins				
	Cytosolic fraction		Membrane fraction		
Mutant	Upregulated	Downregulated	Upregulated	Downregulated	Common in cytosolic and membrane fractions
Δ*mntR*	14	14	6	1	2
Δ*zur*	20	16	18	10	9

were not identified in the membrane or cytosolic subfraction (Table S1), suggesting that their levels were too low to be detected under our conditions. Three proteins involved in metal ion homeostasis, ZagA, DhbB, and DhbF, were increased. The ZagA zinc metallochaperone is encoded by a Zur-regulated gene (34). DhbB and DhbF are involved in biosynthesis of the catecholate siderophore bacillibactin. The *dhbABCDF* operon belongs to the Fur regulon (35), whose transcriptional expression has been shown to weakly decrease in an *mntR* mutant (19). Under our conditions, we assumed

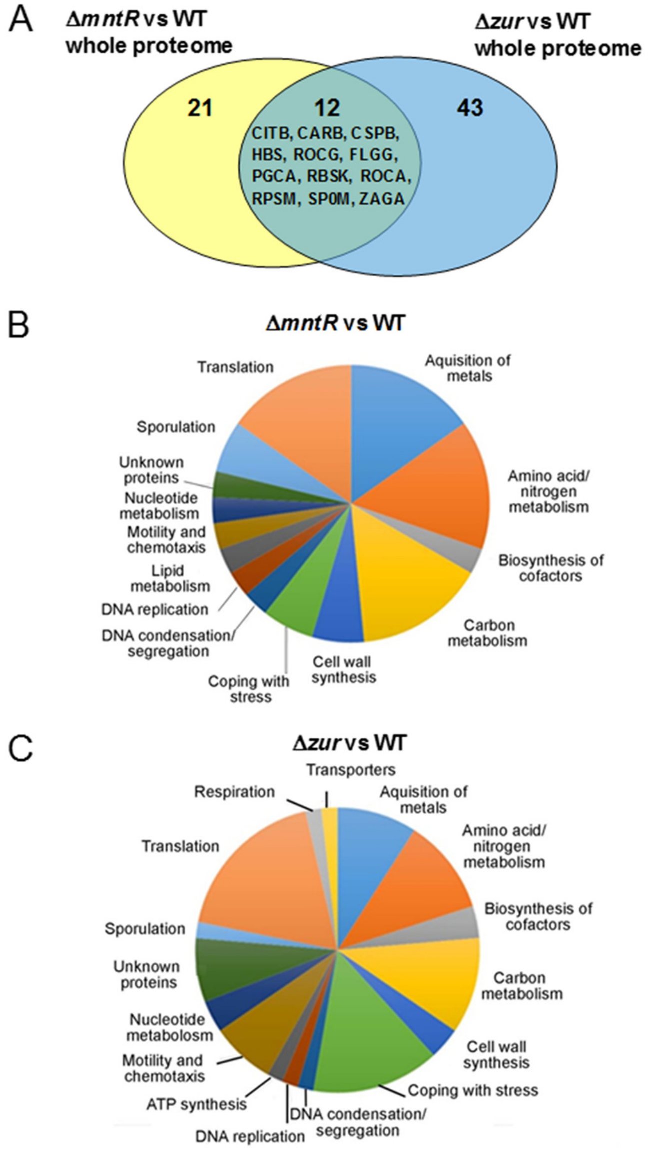

FIG 1 Functional classification of proteins with altered abundance in the *B. subtilis* Δ*mntR* and Δ*zur* mutants. (A) Venn diagram of the 76 proteins showing significant abundance changes between Δ*mntR*, Δ*zur*, and WT cells. (B and C) Proteins are classified according to their involvement in biological processes.

TABLE 3 Proteins differentially abundant in the *B. subtilis* Δ*mntR* mutant

Protein	Fold change in abundance in Δ*mntR* vs wild type	Gene	Function	Functional category[a]
Proteins upregulated in cytosolic fraction				
DhbB[b]	12.75	*dhbB*	Isochorismatase	Acquisition of iron
CitB	10.5	*citB*	Aconitase	TCA cycle
BglH	9.25	*bglH*	Phospho-beta-glucosidase	Utilization of salicin
Spo0M	9.25	*spo0M*	Sporulation	Sporulation
PgcA	8.25	*pgcA*	Alpha-phosphoglucomutase	Biosynthesis of teichoic acid
RocA	7.25	*rocA*	3-Hydroxy-1-pyrroline-5-carboxylate dehydrogenase	Arginine utilization/nitrogen metabolism
RbsK	7	*rbsK*	Ribokinase	Utilization of ribose
MntA[b]	6.75	*mntA*	Manganese ABC transporter	Acquisition of manganese
Syv	6.5	*valS*	Valyl-tRNA synthetase	Translation
Mao4	6.25	*ytsJ*	NADP-dependent malate dehydrogenase	Utilization of malate
Syh	5.75	*hisS*	Histidyl-tRNA synthetase	Translation
RocG[b]	5.25	*rocG*	Glutamate dehydrogenase	Arginine utilization/nitrogen metabolism
MenB	5.25	*menB*	Naphthoate synthase	Biosynthesis of menaquinone
ZagA	5.25	*zagA*	Zinc metallochaperone	Acquisition of zinc
Proteins upregulated in membrane fraction				
DhbF[b]	29	*dhbF*	Involved in bacillibactin biosynthesis	Acquisition of iron
MntA[b]	17.5	*mntA*	Manganese ABC transporter	Acquisition of manganese
MtnK	8.25	*mtnK*	5-Methylthioribose kinase	Methionine metabolism
RocG[b]	7.5	*rocG*	Glutamate dehydrogenase	Arginine utilization/nitrogen metabolism
MntB	6.25	*mntB*	Manganese ABC transporter	Acquisition of manganese
DnaX	5.5	*dnaX*	DNA polymerase III	DNA replication
Proteins downregulated in cytosolic fraction				
RplD	−25.5	*rplD*	Ribosomal protein L4	Translation
CarB	−22.5	*carB*	Carbamoyl-phosphate transferase-arginine	Biosynthesis of arginine
CspB	−20.5	*cspB*	RNA chaperone	Cold stress proteins
FabI	−20.5	*fabI*	Enoyl-acyl carrier protein reductase	Fatty acid biosynthesis
YpfD	−11.5	*ypfD*	Similar to ribosomal protein S1	Translation
SodM	−11	*sodA*	Superoxide dismutase	Resistance against oxidative stress
YkaA	−9.75	*ykaA*	Unknown	Proteins of unknown function
PunA	−8.75	*pupG*	Purine nucleoside phosphorylase	Nucleotide metabolism
RpsM	−8.25	*rpsM*	Ribosomal protein S13	Translation
OppA	−7.25	*oppA*	Oligopeptide ABC transporter	Utilization of peptides
PtsG	−6.5	*ptsG*	Glucose permease	Carbon core metabolism
Hbs	−6.25	*hbs*	Nonspecific DNA-binding protein	DNA condensation/segregation
AsnB	−6	*asnB*	Asparagine synthase	Control of peptidoglycan hydrolysis
PbpC	−6	*pbpC*	Penicillin-binding protein 3	Cell wall synthesis
Protein downregulated in membrane fraction: FlgG	−5.75	*flgE*	Flagellar hook protein	Motility and chemotaxis

[a]According to the SubtiWiki database (77).
[b]Protein detected in both cytosolic and membrane fractions.

that mismetallation of Fur occurs in Δ*mntR* cells, which would lead to increased expression of the *dhb* operon. Interestingly, the SodA Mn-dependent superoxide dismutase was less abundant in Δ*mntR* cells, while two increased proteins, YtsJ and RbsK, participate in metabolic pathways generating NADPH (Table 3). The malic enzyme YtsJ was proposed to be important to balance the intracellular redox pool (36, 37). The ribokinase RbsK belongs to the pentose phosphate (PP) pathway, which yields two molecules of NADPH per glucose molecule (38, 39). NADPH is the unique provider of reducing equivalents to maintain or regenerate bacterial detoxifying and antioxidative defense systems (40). One can hypothesize that Δ*mntR* cells need NADPH to cope with internal oxidative stress and therefore need a metabolic adaptation to maintain the NADPH/$NADP^+$ ratio. However, we observed that *mntR* and *zur* deletions were accompanied by maintained levels of the NADPH/$NADP^+$ ratio during the exponential phase, without significant increase in the NADPH level (data not shown).

Proteomic analysis of the Δ*zur* mutant indicated higher levels of proteins (AdcA, AdcC, FolE2, RpmE2, YciB, ZagA, and ZinT) encoded by Zur-regulated genes, as expected (Table 4). We also observed increased amounts of the CadA efflux ATPase, which is involved in zinc and cadmium metal export (22). The Δ*zur* strain displayed reduced levels of proteins related to stress resistance (Table 4): (i) the bacilliredoxin YqiW (renamed BrxB) promotes a redox switch in response to oxidative stress (41); (ii) the membrane protein YceD, similar to a tellurium resistance protein, is required for survival under ethanol stress (42); and (iii) LiaH is involved in resistance to envelope stress conditions (43). Therefore, the proteomic data suggest that Δ*zur* cells could be more sensitive to environmental stresses. Interestingly, the molecular chaperone DnaK was significantly increased in Δ*zur* cells. DnaK contributes to membrane and overall cell recovery under different stress conditions (44–46), suggesting that the Δ*zur* strain faces internal stress conditions. Finally, the WapA tRNase toxin-WapI antitoxin system (47) was derepressed in the Δ*zur* strain compared to the wild-type strain. Increased expression of WapA (the putative toxin) and decreased expression of WapI (the antitoxin) indicate that Δ*zur* cells may be more susceptible to growth inhibition than wild-type cells.

The proteomic analysis revealed elevated levels of proteins related to the arginine utilization pathway (RocA, RocD, and RocG) in Δ*mntR* and Δ*zur* cells. The *rocABC*, *rocDEF*, and *rocG* operons are under the transcriptional control of RocR and are induced by the presence of arginine, ornithine, or proline in the growth medium. In contrast, expression of *rocE* and *rocD* was repressed in the transcriptomic profile of a *zur* mutant (12). The relationship between Zur and the RocR regulon is not clear. However, our result reinforced the idea that alteration of zinc homeostasis affects expression of the RocR regulon.

Finally, we observed changes in the levels of proteins involved in peptidoglycan synthesis or hydrolysis as well as those involved in the biosynthesis of teichoic acid (Tables 3 and 4). This set includes PgcA, PbpC, and AsnB in Δ*mntR* cells and AsnB, GgaB, GlmU, MurG, and PgcA in Δ*zur* cells. This suggested a possible impact of *mntR* and *zur* deletions on the cell wall structure.

Interestingly, the global proteomics analysis brought new data and revealed some unexpected regulatory effects in the Δ*mntR* and Δ*zur* mutants. It is well known that mRNA and protein expression levels may differ despite being quantified in the same bacterial cells and under similar conditions (48). Previous transcriptomic studies of *zur* and *mntR* mutants in Luria-Bertani (LB) medium identified mainly genes belonging to the Zur and MntR regulons, respectively (12, 19). Our data highlighted a broader impact of *mntR* and *zur* deletions on proteins whose levels are modified in response to perturbation of cellular metal ion pools.

Disruption of metal homeostasis in Δ*mntR* and Δ*zur* mutants. To verify whether deletion of *mntR* or *zur* modifies the cellular metal ion pool, total cell-associated metal ions were quantified in the wild-type, Δ*mntR* and Δ*zur* strains. For this, mid-exponential-phase cells were cultivated at the same optical density at 600 nm (OD_{600}) in LB medium and analyzed by inductively coupled plasma mass spectrometry (ICP-MS).

The Δ*mntR* mutant displayed 2-, ~1.5-, ~1.5-, and ~1.2-fold increases in the levels of Mg^{2+}, Mn^{2+}, Zn^{2+}, and Cd^{2+}, respectively, compared to the wild type (Table 5). In contrast, levels of Fe^{2+}, Co^{2+}, Cu^{2+}, and Ni^{2+} were similar in both strains. Manganese accumulation in Δ*mntR* cells despite activation of efflux systems (21) may indicate that *B. subtilis* tolerates a mild Mn^{2+} intracellular increase without intoxication. The increased level of Cd^{2+} correlates with the higher level of the MntH transporter, which imports both Mn^{2+} and Cd^{2+} ions (18). Accumulation of Zn^{2+} and Mg^{2+} in a Δ*mntR* mutant was unexpected.

The Δ*zur* mutant displayed a 1.5-fold-increased Cu^{2+} level and a 2-fold-decreased Cd^{2+} level compared to the wild type (Table 5). The Δ*zur* mutant had no significant differences in total Mn^{2+}, Zn^{2+}, Mg^{2+}, Fe^{2+}, Co^{2+}, and Ni^{2+} levels. As the internal Zn^{2+} concentration was maintained in Δ*zur* cells, *B. subtilis* appeared to tightly control the

TABLE 4 Proteins differentially abundant in the *B. subtilis* Δ*zur* mutant

Protein	Fold change in abundance in Δ*zur* vs WT	Gene	Function	Functional category[a]
Proteins upregulated in cytosolic fraction				
ZagA[b]	243	*zagA*	Zinc metallochaperone	Acquisition of zinc
AdcA[b]	34	*znuA*	ABC transporter for zinc	Acquisition of zinc
FolE2[b]	22.25	*folE2*	GTP cyclohydrolase IB	Biosynthesis of folate
CarB	18	*carB*	Carbamoyl-phosphate transferase-arginine	Biosynthesis of arginine
DnaK	15.5	*dnaK*	Molecular chaperone	Protein quality control
RocA	14.25	*rocA*	3-Hydroxy-1-pyrroline-5-carboxylate dehydrogenase	Arginine utilization/nitrogen metabolism
AcoN	10.5	*citB*	Aconitase	TCA cycle
ZinT[b]	8	*zinT*	Zinc-binding protein	Acquisition of zinc
GlmU	7.75	*glmU*	Bifunctional *N*-acetylglucosamine-1-phosphate	Biosynthesis of peptidoglycan
RbsK	7.25	*rbsK*	Ribokinase	Utilization of ribose
PgcA	7.25	*pgcA*	Alpha-phosphoglucomutase	Biosynthesis of teichoic acid
Syi	7.25	*ileS*	Isoleucyl-tRNA synthetase	Translation
Fbp	7	*fbp*	Fructose-1,6-bisphosphatase	Gluconeogenesis
GndA	7	*gndA*	NADP-dependent phosphogluconate dehydrogenase	Pentose phosphate pathway
Oat[b]	7	*rocD*	Ornithine transaminase	Ornithine utilization/nitrogen metabolism
PyrG[b]	6.75	*pyrG*	CTP synthase	Nucleotide metabolism
RocG[b]	6.25	*rocG*	Glutamate dehydrogenase	Arginine utilization/nitrogen metabolism
AdcC[b]	5.75	*znuC*	ABC transporter for zinc	Acquisition of zinc
Rl31B	5.5	*rpmE2*	Accessory ribosomal protein	Translation
Sya	5.5	*alaS*	Alanine-tRNA synthetase	Translation
Proteins upregulated in membrane fraction				
ZagA[b]	184.75	*zagA*	Zinc metallochaperone	Acquisition of zinc
AdcA[b]	100.75	*znuA*	ABC transporter for zinc	Acquisition of zinc
YjlD	29.25	*ndh*	NADH dehydrogenase	Respiration
GlpK	28.25	*glpK*	Glycerol kinase	Utilization of glycerol
MetK	22.75	*metK*	*S*-Adenosylmethionine synthetase	Methionine metabolism
ZinT[b]	19.25	*zinT*	Zinc-binding protein	Acquisition of zinc
AdcC[b]	16.75	*znuC*	ABC transporter for zinc	Acquisition of zinc
WapA	15.5	*wapA*	Cell wall-associated protein precursor	Toxins, antitoxins, and immunity against toxins
AsnB	14.75	*asnB*	Asparagine synthase	Control of peptidoglycan hydrolysis
FolE2[b]	12.25	*folE2*	GTP cyclohydrolase IB	Biosynthesis of folate
PyrG[b]	11	*pyrG*	CTP synthase	Nucleotide metabolism
CadA	10	*cadA*	Cadmium transporting ATPase	Resistance against toxic metals
YciB	8.5	*yciB*	Putative L,D-transpeptidase	Acquisition of zinc
Oat[b]	7.75	*rocD*	Ornithine transaminase	Ornithine utilization/nitrogen metabolism
MurG	6.75	*murG*	Peptidoglycan precursor biosynthesis	Biosynthesis of peptidoglycan
RocG[b]	6.75	*rocG*	Glutamate dehydrogenase	Arginine utilization/nitrogen metabolism
Smc	6.25	*smc*	Segregation of replication origins	DNA condensation/segregation
DnaN	5.5	*dnaN*	DNA polymerase III	DNA replication
Proteins downregulated in cytosolic fraction				
Rl7	−46.75	*rplL*	Ribosomal protein L12	Translation
CspB	−37.25	*cspB*	RNA chaperone	Cold stress proteins
Tkt	−25.75	*tkt*	Transketolase	Pentose phosphate pathway
Rs6	−10.5	*rpsF*	Ribosomal protein S6	Translation
RpsM	−10	*rpsM*	Ribosomal protein S13	Translation
Hbs	−9	*hbs*	Nonspecific DNA-binding protein	DNA condensation/segregation
YqiW	−7	*yqiW*	Bacilliredoxin	Resistance against oxidative stress
YjlC[b]	−7	*yjlC*	Unknown	Protein of unknown function
YxkC	−6.5	*yxkC*	Unknown	Protein of unknown function
WapI	−6.25	*wapI*	Immunity protein	Toxins, antitoxins, and immunity against toxins
PthP	−6	*ptsH*	Phosphotransferase system-dependent sugar transport and carbon catabolite repression	Transporters
Rl15	−6	*rplO*	Ribosomal protein L15	Translation
YceD	−5.75	*yceD*	Similar to tellurium resistance protein	Resistance against toxic metals
Rl10	−5.5	*rplJ*	Ribosomal protein L10	Translation
Rs19	−5.5	*rpsS*	Ribosomal protein S19	Translation
YqeY	−5.25	*yqeY*	Unknown	Protein of unknown function

(Continued on next page)

TABLE 4 (Continued)

Protein	Fold change in abundance in Δ*zur* vs WT	Gene	Function	Functional category[a]
Proteins down-regulated in membrane fraction				
Fla	−85	*hag*	Flagellin protein	Motility and chemotaxis
Rs8	−18.25	*rpsH*	Ribosomal protein S8	Translation
CheA	−8.5	*cheA*	Two-component sensor kinase	Motility and chemotaxis
YjlC[b]	−8	*yjlC*	Unknown	Protein of unknown function
AtpF	−7.5	*atpF*	ATP synthase	ATP synthesis
FliL	−6.5	*fliL*	Flagellar protein	Motility and chemotaxis
LiaH	−6	*liaH*	Phage shock-like protein	Resistance against oxidative stress and cell wall antibiotics
Spo0M	−6	*spo0M*	Unknown	Sporulation
FlgG	−5.5	*flgE*	Flagellar hook protein	Motility and chemotaxis
GgaB	−5	*ggaB*	Membrane protein	Biosynthesis of teichoic acid

[a]According to the SubtiWiki database (77).
[b]Protein detected in both cytosolic and membrane fractions.

level of Zn^{2+} to avoid zinc intoxication. Copper accumulation in a Δ*zur* mutant was intriguing. In *B. subtilis*, copper uptake involves a well-defined transporter, YcnJ, whose synthesis responds to copper availability (49). The lower level of Cd^{2+} detected in Δ*zur* cells was in line with increased CadA, the major determinant for Cd^{2+} resistance (Table 4). In zinc excess, CzrA binds Zn^{2+} to trigger derepression of CadA (22, 50).

Differential Mg^{2+}-dependent growth of Δ*zur* and Δ*mntR* cells. We detected an intracellular Mg^{2+} concentration of ~0.5 to 1.0 mM in the three *B. subtilis* strains (Table 5). To gain insight into the physiological relevance of Mg^{2+} accumulation in the Δ*mntR* strain, growth assays were performed under conditions of Mg^{2+} starvation. Precultures of the wild-type, Δ*mntR*, and Δ*zur* strains in LB medium were inoculated in M9 defined medium in the presence or absence of Mg^{2+}. In M9 medium containing 25 mM Mg^{2+}, all strains grew with similar growth kinetics (Fig. 2A). In Mg^{2+}-depleted M9 medium (containing only traces of Mg^{2+}), only the Δ*mntR* mutant showed a growth benefit (Fig. 2B). Therefore, Mg^{2+} accumulation in Δ*mntR* cells grown in LB medium appeared to be effective to support growth in Mg^{2+}-depleted M9 medium. It is worth noting that supplementation of growth media with 5 to 25 mM Mg^{2+} may suppress morphological and vital defects of several *B. subtilis* mutants with mutations in cell wall-related genes (e.g., *ponA*, *ugtP*, *pgcA*, *gtaB*, or *asnB*) (51, 52), but the mechanisms underlying this rescuing role are still unknown. At present, we cannot explain how intracellular Mg^{2+} compensates for the absence of external Mg^{2+} ions.

Sensitivity of Δ*mntR* and Δ*zur* cells to environmental stresses. As the proteomic analysis revealed that Δ*zur* cells displayed reduced levels of proteins related to stress resistance (BrxB, YceD, and LiaH), we tested whether environmental stresses such as organic solvent and increased salinity could affect growth of Δ*zur* and Δ*mntR* cells compared to that of the wild type. Growing bacteria were exposed to a final sublethal concentration of 4% (vol/vol) ethanol. Under the conditions used, no effect on the

TABLE 5 Metal content of *B. subtilis* wild type, Δ*mntR* and Δ*zur* cells measured by ICP-MS

	Concn (μM)[a] in:		
Metal ion	WT	Δ*mntR* mutant	Δ*zur* mutant
Fe^{2+}	203 ± 29.2	229.4 ± 39.1	151.1 ± 49.6
Mg^{2+}	523.7 ± 85.5	1,155.5 ± 166.8	621.3 ± 70.1
Mn^{2+}	26.4 ± 3.1	42.1 ± 6.4	28 ± 4.5
Zn^{2+}	224.3 ± 25.1	302.7 ± 28.5	237.6 ± 32.7
Cd^{2+}	2.8 ± 0.2	3.6 ± 0.4	1.4 ± 0.3
Co^{2+}	0.25 ± 0.15	0.18 ± 0.1	0.18 ± 0.1
Cu^{2+}	6.2 ± 0.6	6.5 ± 0.6	8.8 ± 1.4
Ni^{2+}	6.4 ± 1.1	7.1 ± 1.4	7.5 ± 1.6

[a]Results are means ± standard deviations.

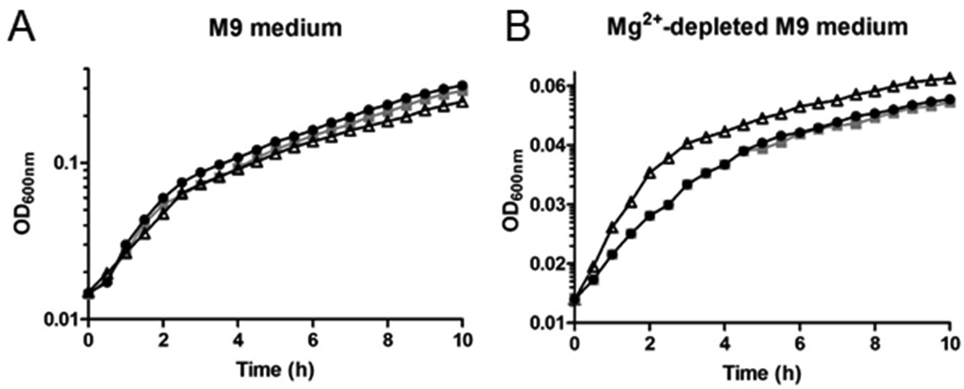

FIG 2 Effect of magnesium starvation on growth of wild-type, Δ*mntR*, and Δ*zur* cells. (A) Growth curves of the wild-type (black symbols), Δ*mntR* (white symbols), and Δ*zur* (gray symbols) strains grown in M9 medium in the presence of 25 mM $MgCl_2$. A representative assay is represented. (B) Growth curves of the wild-type (black symbols), Δ*mntR* (white symbols), and Δ*zur* (gray symbols) strains grown in $MgCl_2$-depleted M9 medium. The doubling time of wild-type and Δ*zur* cells is approximately 208 min. The doubling time of Δ*mntR* cells is approximately 122 min. A representative assay is represented. Note that the *x* axes are different in panels A and B for a better view of the data.

growth rate was observed for the wild-type cells, whereas 4% ethanol transiently affected growth of the Δ*zur* and Δ*mntR* cells (Fig. 3A and B). The direct target of ethanol is the membrane bilayer. A lower resistance to ethanol exposure suggests that Δ*zur* and Δ*mntR* cells are less efficient in activating an early response to stress and/or that their

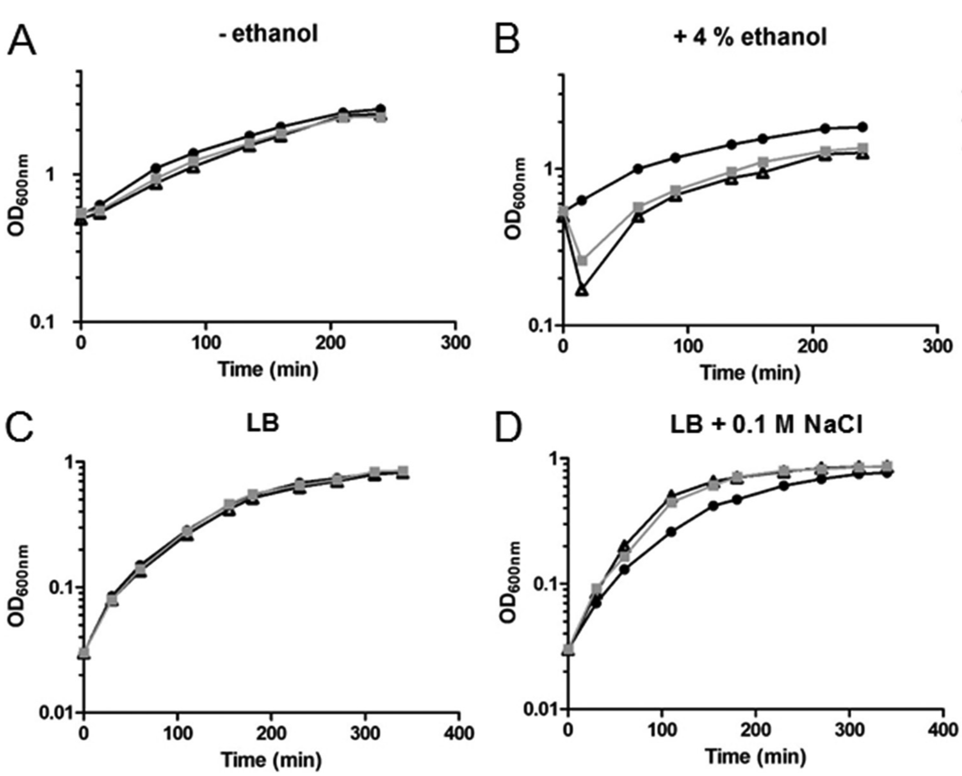

FIG 3 Effects of ethanol and NaCl stresses on growth of wild-type, Δ*mntR*, and Δ*zur* cells. (A) Growth curves of the wild-type (black symbols), Δ*mntR* (white symbols), and Δ*zur* (gray symbols) strains grown in LB medium without ethanol addition. A representative assay is represented. (B) Growth curves of the wild-type (circles), Δ*mntR* (triangles), and Δ*zur* (squares) strains grown in LB medium after addition of 4% ethanol (final concentration) at an OD_{600} of 0.6. A representative assay is represented. (C) Growth curves of the wild-type (black symbols), Δ*mntR* (white symbols), and Δ*zur* (gray symbols) strains grown in LB medium without NaCl addition. A representative assay is represented. (D) Growth curves of the wild-type (circles), Δ*mntR* (triangles), and Δ*zur* (squares) strains grown in LB medium with addition of NaCl at 0.1 M. A representative assay is represented.

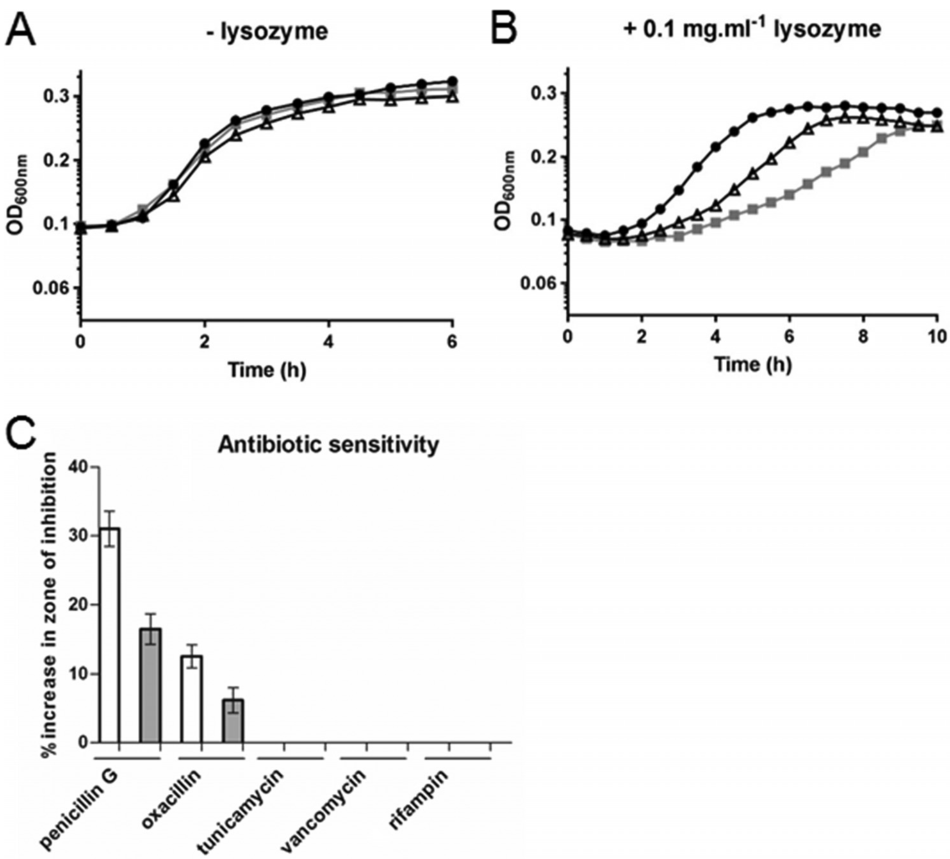

FIG 4 Increased sensitivity of the Δ*mntR* and Δ*zur* mutants to lysozyme and antibiotics. (A) Growth curves of the wild-type (black symbols), Δ*mntR* (triangles), and Δ*zur* (gray symbols) strains grown in LB medium. A representative assay is represented. (B) Growth curves of the wild-type (circles), Δ*mntR* (triangles), and Δ*zur* (squares) strains grown in LB medium in the presence of 1 mg · ml^{-1} lysozyme. A representative assay is represented. (C) Results of disk diffusion assays with the indicated antibiotics. Bars indicate the percent increase in zone of inhibition for the Δ*mntR* (white bars) and Δ*zur* (gray bars) mutants relative to the wild type. All the experiments were performed at least in three biological replicates.

membrane lipids and proteins differ from those in the wild-type cells. Remarkably, we observed in Δ*mntR* cells a 20-fold-decreased amount of the FabI protein, which is involved in fatty acid biosynthesis (Table 3).

We further tested the effect of NaCl on growth. A moderate saline stress was imposed by incubation of the cells in the presence of 0.1 M NaCl. Under these conditions, we observed a slight but reproducible enhanced fitness of the Δ*zur* and Δ*mntR* strains compared to the wild-type strain (Fig. 3C and D). No difference in resistance was observed with 0.5 M NaCl (data not shown). As bacterial responses to osmotic challenges are very complex, it is not obvious how the Δ*mntR* and Δ*zur* strains are better suited than the wild type to cope with moderate saline stress.

Sensitivity of Δ*mntR* and Δ*zur* cells to lysozyme and beta-lactam antibiotics. The proteomic analysis revealed modified levels of proteins (AsnB, GlmU, and MurG) involved in peptidoglycan biosynthesis in Δ*mntR* and Δ*zur* cells. To test whether *mntR* and *zur* deletions modified the peptidoglycan integrity, bacteria were treated with lysozyme. Both the Δ*mntR* and Δ*zur* mutants were more sensitive to 0.1 mg · ml^{-1} lysozyme than the wild-type strain (Fig. 4A and B). With 0.5 mg · ml^{-1} lysozyme, Δ*mntR*, Δ*zur*, and wild-type cells showed similar growth defects (data not shown). In addition, a disk diffusion assay was performed to compare the sensitivities of the mutant and wild-type strains to several antibiotics. The Δ*mntR* and Δ*zur* mutants were more sensitive than the wild-type strain to penicillin G and oxacillin, which inhibit formation of peptidoglycan cross-links in the bacterial cell wall (Fig. 4C). In contrast, the two mutants had the same sensitivity as the wild-type strain to vancomycin and to tunicamycin, which target other steps of cell wall synthesis, and to the RNA polymerase inhibitor rifampin. The decreased resistance of the Δ*mntR* and Δ*zur* strains to lysozyme and beta-lactam antibiotics strongly suggests that structural modifications take place in the cell wall of mutant cells. This is in line with the (above-described) proteomic analysis, which indicated deregulation of proteins involved in cell wall plasticity.

Bacterial interfacial potential and cell wall thickness are altered in Δ*mntR* and Δ*zur* mutants. Modifications in cell wall composition are expected to affect bacterial surface charge (53, 54). We performed zeta potential measurements to determine bacterial surface potentials. The zeta potential indicates an electrochemical property of the bacterial cell surface which represents the transmembrane potential that maintains the cell wall/membrane architecture. Negative zeta potentials were measured for all three strains grown in LB medium, as expected for Gram-positive bacteria, which contain negatively charged teichoic acids. However, the Δ*mntR* mutant exhibited a lesser negative potential (-11.6 ± 0.4 mV) than the wild type (-13.5 ± 0.3 mV) and Δ*zur* (-13.8 ± 0.7 mV) cells. This finding suggests that deletion of the *mntR* gene alters cell surface permeability, as a correlation between negative zeta potential and membrane integrity was previously shown (55). It should be noted that proteomic analysis indicated increased levels of PgcA, a protein involved in biosynthesis of teichoic acid that also may modify the surface charge of bacteria.

To further identify the modifications that differentiate the cell walls of Δ*mntR* and Δ*zur* cells, cultures grown in LB were collected at mid-exponential phase and observed in thin cross-section by transmission electron microscopy (TEM). Bacterial cells of the 3 strains appeared as well-separated bacilli (Fig. 5A). The cell wall of the Δ*zur* mutant was thinner (32 ± 4.5 nm) than that of the parental strain (38 ± 3.6 nm) (Fig. 5A and B). In contrast, the cell wall thickness of the Δ*mntR* mutant was greater (42 ± 3.5 nm) than that of the wild type. We assumed that alteration of cell wall thickness in the Δ*mntR* and Δ*zur* mutants and modification of the zeta potential in Δ*mntR* cells resulted from changes in cell surface composition and/or structure. The interplay between manganese and zinc homeostasis and the proteins involved in cell wall plasticity identified in the proteomic approach (Tables 3 and 4) deserves future investigation.

Low $O_2^{\cdot -}$ and H_2O_2 accumulation in Δ*mntR* and Δ*zur* mutants. Neutralization of the surface potential of bacteria was shown to trigger the production of ROS (53, 56). Modifications in bacterial surface potential may thus result from cell wall adjustments but also from enhanced ROS production within the bacterial cells (53). However, our proteomic data were in favor of reducing ROS levels. Indeed, we observed decreased levels of BrxB and SodA in the Δ*zur* and Δ*mntR* mutants, respectively. The BrxB (bacilliredoxin)- and SodA (Mn-dependent superoxide dismutase)-encoding genes can be induced by oxidative stress. Thus, a lower level of BrxB and SodA might indicate a reduction in intracellular ROS. To verify whether bacterial surface charge modifications resulted from intracellular ROS accumulation, we compared the amounts of $O_2^{\cdot -}$ and H_2O_2 production in Δ*mntR* and Δ*zur* cells to those in the wild-type strain.

The 2,3-bis-(2-methoxy-4-nitro-5-sulfophenyl)-2H-tetrazolium-5-carboxanilide salt (XTT) assay was performed to estimate cellular production of $O_2^{\cdot -}$. No light adsorption was observed for LB medium alone. XTT absorbs light at 470 nm only when reduced by $O_2^{\cdot -}$ and does not do so in its oxidized form. The amount of $O_2^{\cdot -}$ in cells in mid-exponential growth phase in LB medium was lower in Δ*mntR* and Δ*zur* cells than in the wild type (Fig. 6A). The intracellular concentration of H_2O_2 was calculated in bacteria in mid-exponential phase based on the calibration curve obtained with pure H_2O_2 using the Amplex red assay. The generation of H_2O_2 was found to be lower in the mutants than in the wild-type strain (Fig. 6B). The Δ*mntR* and Δ*zur* mutants appeared to accumulate less intracellular ROS than the wild-type strain. We thus propose that the modification in the bacterial surface potential in Δ*mntR* cells could result from changes in the cell wall structure rather than from intracellular ROS accumulation.

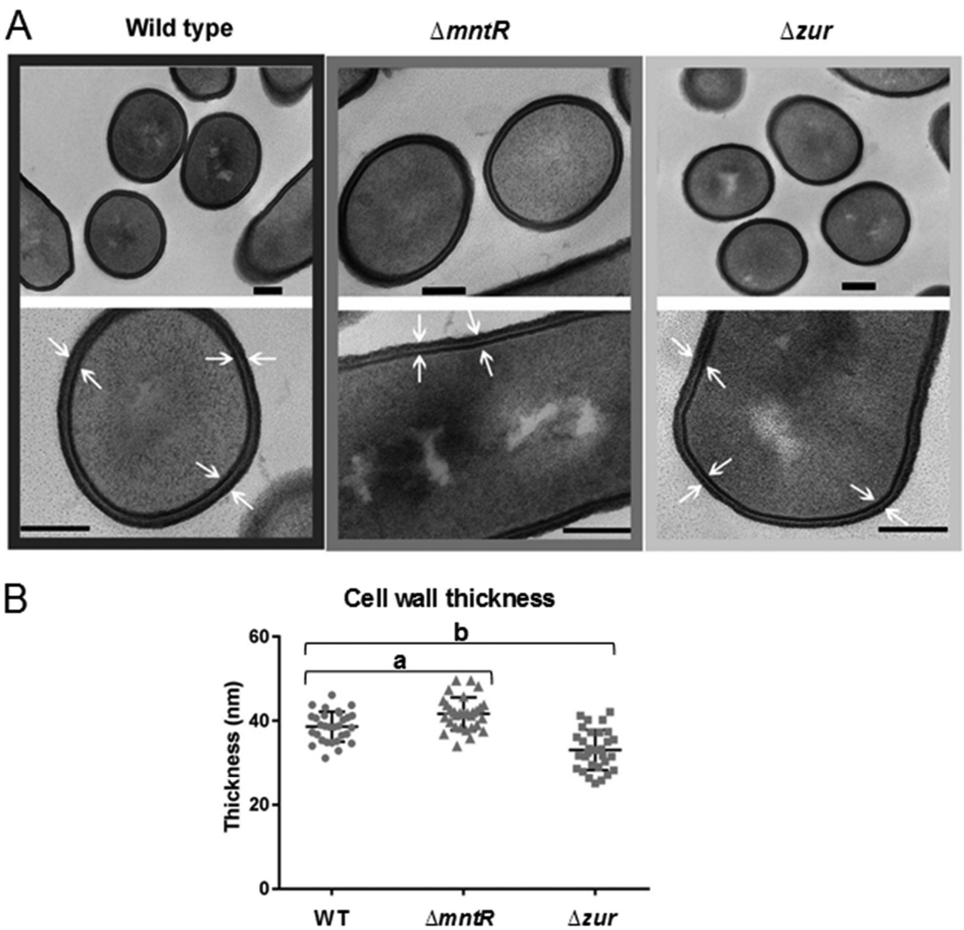

FIG 5 The *mntR* and *zur* deletions are associated with altered cell wall thickness. (A) Transmission electron microscopy images of representative cells of wild-type, Δ*mntR*, and Δ*zur* cells during mid-log growth phase. Bars, 100 nm. (B) Dot blot graph of the cell wall thickness. Each dot represents a measurement for a single bacillus. a, $P = 1.8 \cdot 10^{-4} < 0.05$; b, $P = 4.4 \cdot 10^{-6} < 0.05$.

Effect of external H_2O_2 on Δ*mntR* and Δ*zur* cells. To estimate bacterial sensitivity to external oxidative stress, we compared the survival of wild-type, Δ*mntR*, and Δ*zur* cells when challenged with external H_2O_2. Disk diffusion assays indicated an increase in the zone of growth inhibition for the Δ*mntR* and Δ*zur* mutants compared to that for the wild-type strain (Fig. 6C). Similarly, both the Δ*mntR* and Δ*zur* mutants showed a growth defect compared to the wild-type strain when exposed to 50 or 100 μM H_2O_2 for 15 min in LB medium (Fig. 6D). Increased sensitivity of the Δ*mntR* mutant to H_2O_2 correlates with the role of Mn^{2+} as corepressor of the PerR regulator in response to peroxide stress (57–60). Increased susceptibility of the Δ*zur* mutant to H_2O_2 suggests that Zur is required for expression of oxidative stress defenses, as observed in *Corynebacterium diphtheriae* (61).

DISCUSSION

Our results provide a new view on *B. subtilis mntR* and *zur* mutants under stress-related conditions. Proteomic analysis revealed 33 and 55 proteins whose abundance was affected in Δ*mntR* and Δ*zur* mutants, respectively. The identified proteins are involved in various cellular processes, notably in translation, amino acid/nitrogen/carbon metabolism, and cell wall homeostasis. Commonly affected proteins suggest coordination between the MntR and Zur regulatory networks.

The Δ*mntR* and Δ*zur* mutants displayed growth kinetics similar to those of the parental strain, although intracellular pools of some essential metal ions differed (Table 5). The

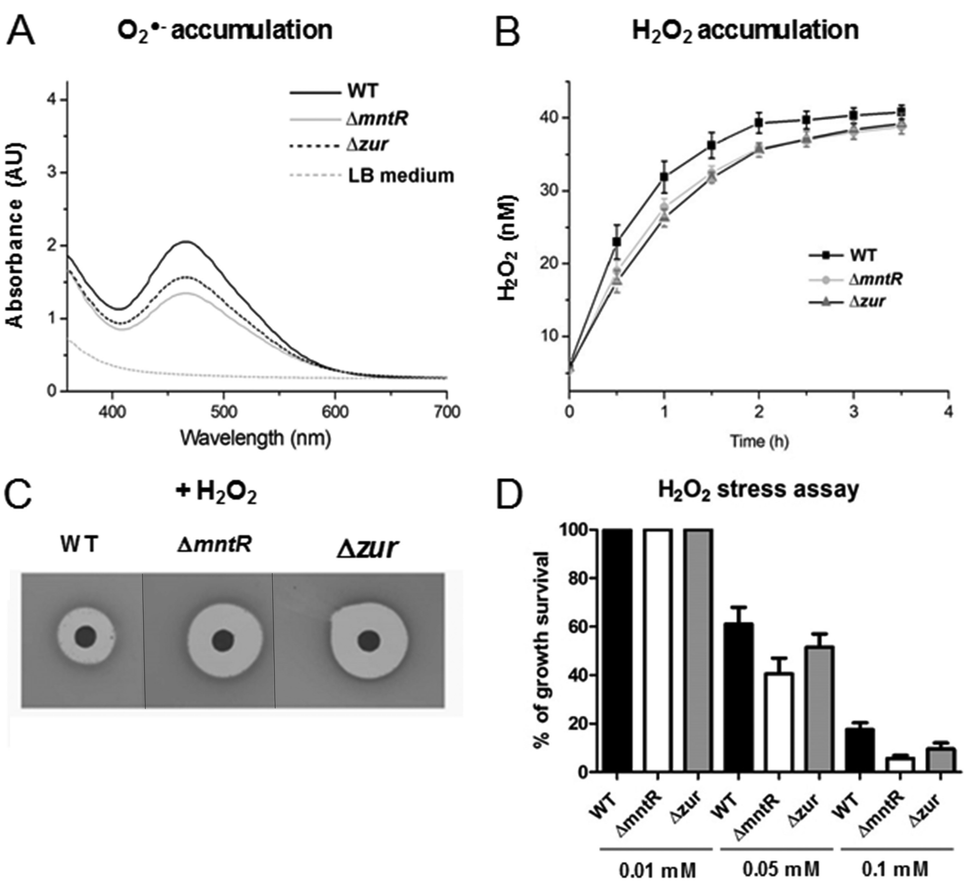

FIG 6 ROS accumulation and oxidative stress assays in Δ*mntR* and Δ*zur* mutants. (A) Quantification of $O_2^{\cdot -}$ produced in wild-type (WT), Δ*mntR*, and Δ*zur* cells at an OD_{600} of 1 in LB medium. (B) Quantification of H_2O_2 produced in WT, Δ*mntR*, and Δ*zur* cells during 4 h of growth in LB medium. (C) Plates from a disk diffusion assay with a drop of 3 M hydrogen peroxide (H_2O_2). (D) The histograms represent the percentage of survival of WT, Δ*mntR*, and Δ*zur* cells at 15 min after addition of 0.01, 0.05, or 0.1 mM H_2O_2. The survival rate was determined as the ratio of the number of CFU per milliliter after 15 min to the number of CFU per milliliter before addition of H_2O_2.

1.5-fold-greater accumulation of Mn^{2+} in the Δ*mntR* mutant versus the WT indicates that *B. subtilis* can tolerate an intracellular increase in Mn^{2+} without bacterial growth being affected. In contrast, maintenance of the Zn^{2+} content in a Δ*zur* mutant provides evidence that alternative pathways can maintain intracellular Zn^{2+} homeostasis. Surprisingly, Mg^{2+} and Zn^{2+} metal ions also accumulate in the Δ*mntR* mutant (2.2-fold and 1.4-fold increased, respectively), while Cu^{2+} accumulates 1.5-fold in Δ*zur* cells. It is possible that metabolic changes in Δ*mntR* and Δ*zur* cells provoke secondary demands for other metal ions, leading to their increased levels. How bacteria simultaneously regulate the content of multiple metal ions merits further studies.

Metal ions catalyze numerous metabolic processes by their roles in electron transfer. Essential pathways such as the tricarboxylic acid (TCA) cycle (CitB) and the stringent response are impacted by bacterial metabolic status (62–65). Our proteomic analyses revealed higher levels of RocA, RocD, and RocG proteins in both Δ*mntR* and Δ*zur* mutants. These enzymes are involved in arginine and ornithine utilization to generate ammonium and may contribute to maintaining intracellular pH homeostasis (66).

We previously performed a genome-wide identification of Zur-binding sites by chromatin immunoprecipitation coupled with hybridization to DNA tiling arrays (ChIP-on-chip) (31). We were initially surprised that promoters identified by ChIP-on-chip did not match proteins identified in the Δ*zur* mutant. However, the differences may be explained by the importance of posttranscriptional control of translation, as well as the effects of transcriptional regulators other than Zur in controlling gene expression.

We showed that the Δ*mntR* and Δ*zur* mutants accumulate less ROS (e.g., $O_2^{\cdot-}$ and H_2O_2) than the wild-type counterpart (Fig. 6). Mn^{2+} and Zn^{2+} metal ions are intimately linked to the ability to withstand ROS. Mn^{2+} itself or in a complex with a cellular component is involved in cellular defense against $O_2^{\cdot-}$ stress and can therefore substitute for SodA (67). An elevated extracellular Zn^{2+} amount protects *B. subtilis* from peroxide stress (59). Hence, slight increases in Mn^{2+} and Zn^{2+} pools in Δ*mntR* cells (Table 5) may sufficiently promote the antioxidative defense mechanism to diminish the need for Mn-dependent superoxide dismutase SodA (Table 3). It is intriguing that the Δ*zur* mutant shows a similar decrease of ROS, whereas the Mn^{2+} and Zn^{2+} levels are not modified (Table 5 and Fig. 6). This raises questions about the regulatory role of Zur in maintaining redox potential.

Remarkably, deletion of *mntR* or *zur* enhanced sensitivity to lysozyme and beta-lactam antibiotics, both of which target the cell wall (Fig. 4). Our results and previous studies suggest mechanisms that may explain these findings. First, increased sensitivity to peptidoglycan synthesis inhibitors can be due to modification of the cell wall structure and/or composition in the mutants. Our findings are in line with this, since the cell wall thickness and bacterial surface zeta potential were modified in the Δ*mntR* and Δ*zur* mutants compared to the wild-type strain (Fig. 5). Second, beta-lactam antibiotics were proposed to generate ROS that contribute to bacterial death (68). We observed a greater sensitivity to external ROS of Δ*mntR* and Δ*zur* cells than of the wild-type strain (Fig. 6). Third, there is an intimate connection between metal ions and antibiotic activity Some antibiotics are known to require metal ions for their activity (69). When not required to mediate target binding, interaction of metal ions with antibiotics can provide an additional mode of antibacterial action, as seen, for example, with Zn^{2+}, which potentiates the antibiotic activity of vancomycin (70), and with ZnMgO, which increases ciprofloxacin activity (71). We showed here that Δ*mntR* and Δ*zur* cells accumulate some metal ions (Table 5), which may potentiate antibiotic activity. Further investigations are needed to determine the exact role(s) of Zur and MntR in bacterial sensitivity to antibiotics.

Altogether, this work might uncover new targets for intervention to successfully combat emerging bacterial multiresistance against conventional antibiotics.

MATERIALS AND METHODS

Bacterial strains and growth conditions. The *B. subtilis* strains used in this work are listed in Table 1. *B. subtilis* cells were grown in Luria-Bertani (LB) medium or in M9 minimal medium (72). In media containing NaCl, the concentrations are indicated. Antibiotics were added at the following concentrations when required: 5 μg kanamycin ml^{-1} and 60 μg spectinomycin ml^{-1}. Solid media were prepared by addition of 20 g Noble agar (Difco) $liter^{-1}$. Standard procedures were used to transform *B. subtilis* (73).

DNA manipulations. In PCR, the *Pfu* DNA polymerase was used as recommended by the manufacturer (Biolabs). DNA fragments were purified from agarose gels using the QIAquick kit (Qiagen).

Construction of strains. The *mntR* mutant BSAS46 was constructed by homologous replacement of the *mntR* coding sequence with the kanamycin resistance gene *aphA3* using a joining PCR technique. The *aphA3* gene was first amplified. The region upstream of the *mntR* gene (nucleotides 2542520 to 2543556) was amplified by PCR with a 24-bp *aphA3* fragment at its 3′ end. The region downstream of *mntR* (nucleotides 2543796 to 2544739) was amplified with a 24-bp *aphA3* fragment at its 5′ end. The three DNA fragments were combined, and then a PCR was performed with the two external oligonucleotides. The final product, corresponding to the two regions flanking *mntR* with the inserted *aphA3* cassette in between, was purified from a gel and used to transform *B. subtilis*. Integration and deletion were confirmed by PCR and verified by DNA sequencing.

Intracellular metal concentration measurement by ICP-MS. Overnight cultures of wild-type, Δ*mntR*, and Δ*zur B. subtilis* strains were diluted to an optical density at 600 nm (OD_{600}) of 0.05 in 15 ml of fresh LB medium cultured in 50-ml Falcon tubes. Bacteria were incubated at 37°C until exponential phase (OD_{600} of around 0.8). Cell cultures were centrifuged at 4,000 $\times$ *g* at 4°C for 10 min and washed three times in 5 ml of ultrapure water (Millipore) with EDTA added to 1 mM. Samples were dried overnight at 80°C and then acidified twice with Suprapur 65% nitric acid (Merck Millipore) until mineralization. Samples were further analyzed at the University of Montpellier II (Laboratoire ICP-MS, UMR5543 Géosciences). Samples were dissolved with 250 ml of nitric acid (65%) for 1 h. They were diluted 1,000-fold in double-distilled water and analyzed using an Agilent 7700x quadrupole inductively coupled plasma mass spectrometer. Concentrations were determined by analyzing standard solutions. To obtain the number of atoms of metal ions per cell, the raw data were normalized to the washing solution. The measurement for each strain was performed in three replicates.

Quantification of NADPH and NADP$^+$. Detection and quantification of NADPH and NADP$^+$ content were done using the NADP/NADPH microplate assay kit (Cohesion Biosciences). Assays were performed on cells grown in LB medium until the OD_{600} was around 0.8. Each experiment was performed in three independent replicates.

Effects of ethanol and NaCl. Overnight cultures were diluted in fresh LB medium to an initial OD_{600} of 0.1 and incubated in flasks with shaking (200 rpm) at 37°C. Bacterial growth was measured by following the optical density at 600 nm. In the ethanol stress assay, ethanol at a final concentration of 4% was added when the OD_{600} reached 0.6. In the saline assay, NaCl was added at final concentration of 0.1 M at the beginning of the cultures.

Effects of lysozyme and $MgCl_2$. Overnight cultures were diluted at least 100-fold in fresh medium. Growth curves were done in 96-well plates in a Tecan plate reader (Tecan Infinite M200PRO) with continuous agitation at 37°C. Growth conditions were as indicated elsewhere in the text. At least three independent biological replicates were performed.

Assay of sensitivity to antibiotics. The assay of antibiotic sensitivity was performed on solid media. *B. subtilis* strains were grown in LB medium to an OD_{600} of 1. One milliliter of growing culture was spread onto petri plates containing LB medium. The plates were dried briefly in a laminar flow hood before 5-mm paper disks (Whatman) containing 25 μl of antibiotic solution were placed on the plates (penicillin G, 8 mg · ml^{-1}; oxacillin10, μg · ml^{-1}; tunicamycin, 375 μg · ml^{-1}; vancomycin, 0.5 μg · ml^{-1}). The plates were incubated at 37°C overnight. The zones of inhibition were measured by using ImageJ after scanning the plates. Standard deviations were calculated from three independent assays.

Peroxide stress assays. To perform disk diffusion assays, the cell number was determined in exponential-phase cultures by evaluating the CFU per milliliter. One milliliter of each microbial suspension containing 1×10^8 bacterial cells ml^{-1} (corresponding to a 0.5 McFarland standard) was spread over the surface of the agar plates. The plates were dried briefly in a laminar flow hood. A sterile 5-mm paper disk was placed on the agar surface, and 10 μl of 3 M hydrogen peroxide (H_2O_2) was added to the disk. For the stress assay in liquid medium, cultures were inoculated at an OD_{600} of 0.05 in LB medium and incubated at 37°C with agitation at 200 rpm. At an OD_{600} of 0.5, H_2O_2 was added at 0.1 mM. After 15 min of incubation, serial dilutions were plated on LB agar. The CFU per milliliter were counted. The number of CFU per milliliter before the stress was used as a reference to measure the rate of survival.

Quantification of $O_2^{\cdot -}$ and H_2O_2 free radicals. The bacterial production of superoxide radical ion ($O_2^{\cdot -}$) was evaluated by measuring the adsorption of XTT [2,3-bis-(2-methoxy-4-nitro-5-sulfophenyl)-2H-tetrazolium-5-carboxanilide] (Sigma). XTT was dissolved in PBS (pH 7) and added to the bacterial culture to a final concentration of 0.4 mM. When reduced by $O_2^{\cdot -}$, XTT forms water-soluble XTT-formazan, which adsorbs light at 470 nm. The changes in absorbance at 470 nm were monitored using an Infinite M200 luminescence reader (Tecan, Germany). XTT absorbs light at 470 nm only when reduced by $O_2^{\cdot -}$.

Intracellular production of H_2O_2 was quantified using the Amplex red assay. *B. subtilis* strains were grown in LB medium to mid-exponential phase. After centrifugation, pellets were resuspended in phosphate-buffered saline (PBS) and transferred to a 96-well plate that contained 20 μl of enzymatic mix (1 μl 10-acetyl-3,7-dihydroxyphenoxazine [ADHP] reagent, 1 μl horseradish peroxidase, and 18 μl assay buffer) in each well. Resorufin fluorescence was measured using a spectrofluorometer (Tecan Infinite M200PRO) with excitation and emission wavelengths of 530 and 590 nm, respectively. H_2O_2 calibration was done using H_2O_2 standard solutions ranging from 100 to 1,500 nM. Each experiment was performed in duplicate and repeated at least twice.

Whole-cell surface potential. The zeta potential of the bacterial cell growth in exponential phase in LB medium was measured using a Zetasizer Nano ZS90 instrument (Malvern, UK). The results for zeta potential are presented as the average value from three independent cultures (10 measurements per culture).

TEM. For transmission electron microscopy (TEM), bacterial pellets were collected at an OD_{600} of 1 and fixed with 2% glutaraldehyde in 0.1 m sodium cacodylate buffer, pH 7.2, at room temperature for 3 h. Samples were then contrasted with 0.5% oolong tea extract in sodium cacodylate buffer (74), postfixed with 1% osmium tetroxide containing 1.5% potassium cyanoferrate, gradually dehydrated in ethanol (30% to 100%), substituted gradually in a mixture of propylene oxide and Epon, and embedded in Epon (Delta Microscopy, Labège, France). Thin (70-nm) sections were collected onto 200-mesh copper grids and counterstained with lead citrate. Grids were examined using a Hitachi HT7700 electron microscope operated at 80 kV (Elexience, France). Images were acquired with a charge-coupled device camera (Advanced Microscopy Techniques Corp., Japan). The thickness of the cell wall was measured on TEM micrographs of at least five cells at a magnification of ×70,000, taking at least six measurements on each cell. Statistical analysis was performed with the unpaired Student *t* test, and a P value of <0.05 was considered significant. Analyses were performed using Prism 7 (GraphPad Software, San Diego, CA).

Sample preparation for proteomic analysis. To analyze the proteomic profiles of the wild-type, Δ*mntR*, and Δ*zur* cells, protein extraction and tryptic digestion in gel were performed as described in detail previously (75). Briefly, four independent cultures of each *B. subtilis* strain were grown in LB medium at an OD_{600} of 0.8. Cells were harvested by centrifugation and disrupted by a passage through a One Shot cell disrupter (Constant Systems Ltd., Warwickshire, UK). After centrifugation, the resulting supernatants were ultracentrifuged (100,000 × *g*, 1 h, 4°C). Cytoplasmic fractions were designated the soluble parts after a single ultracentrifugation step. The remaining pellets were considered the crude membrane fraction. The total protein concentration was measured using a NanoDrop instrument. All of the samples were loaded on 10% NuPAGE Bis-Tris gels (Invitrogen). In-gel digestion of the proteins was performed on bands excised from one-dimensional SDS-PAGE gel. The quantity of modified trypsin (Promega, sequencing grade) was 0.5 μg per sample. In the final step, tryptic peptides were resuspended in 25 μl of precolumn loading buffer containing 0.05% (vol/vol) trifluoroacetic acid (TFA) and 5% (vol/vol) acetonitrile prior to LC-MS/MS analysis.

LC-MS. Mass spectrometry was performed on the Plateforme d'Analyse Protéomique de Paris Sud Ouest (PAPPSO) platform as described in detail previously (75). A NanoLC-Ultra Eksigent (Sciex) system connected to a Q-Exactive mass spectrometer (Thermo Fisher) by a nanoelectrospray ion source was used. The protein identification was performed with X!TandemPipeline (open-source software developed by PAPPSO, version 3.3.1) against a *Bacillus subtilis* 168 protein database (4,253 entries). The X!Tandem search parameters were as follows: trypsin specificity with two missed cleavages, fixed alkylation of cysteine (+57.0215), and variable oxidation of methionine (+15.9949). The protein identification was run with a precursor mass tolerance of 10 ppm and a fragment mass tolerance of 0.02 Da. For all proteins identified with a protein E value of <0.01 in the first step, we searched for additional peptides to reinforce identification using similar parameters except that semitryptic peptides and protein N-terminal acetylations were accepted. The final search results were filtered as follows: (i) peptide E value of <0.01 with a minimum of 2 peptides per protein and (ii) protein E value of <0.05.

Relative quantification of peptides and proteins. Peptide were analyzed by spectral counting (SC). SC takes into account the number of assigned spectra for each protein and is correlated to relative protein abundance. For control quality of data, normalization, filtration, and statistical analysis, MassChroqR (http://pappso.inra.fr/bioinfo/masschroqr/) was used. Proteins with fewer than two peptides were removed. Peptides with a variation ratio of <1.5 were eliminated, as were peptides with a standard deviation from the retention time of 20 s and higher. Repeatable peptides were those which were present in at least 7 of 8 samples. The data set was normalized based on the median retention time, and missing peptide intensities and protein abundances were imputed. The proteins whose numbers of peaks were significantly different (with a minimum difference of 5 peaks between the mutant and the wild type) were determined by using the Kruskal-Wallis test. A one-way ANOVA model was used to analyze changes, with the genotype as a fixed effect. A protein was considered significantly variable when the *P* value was <0.05 (see Table S1 in the supplemental material).

Availability of data. All supporting data are included in the main article and in the supplemental material.

SUPPLEMENTAL MATERIAL

Supplemental material is available online only.

SUPPLEMENTAL FILE 1, XLS file, 1.4 MB.

ACKNOWLEDGMENTS

We benefited from the facilities of the MIMA2 MET (GABI, INRA) and PAPSSO (Micalis, INRA) platforms, Jouy en Josas, France. We thank David Portehault (LCMCP, France) for helping with zeta potential measurements. We are grateful to Philippe Noirot for the support to initiate this project. We gratefully acknowledge Alexandra Gruss and Stéphane Aymerich for critical reading of the manuscript.

This research received funding from the European Union, Marie Curie ITN AMBER, 317338.

P.R., J.V., and S.A. conceived and designed the experiments. P.R., J.A.-M., A.G., C.P., J.V., and S.A. performed the experiments. P.R., A.A.-F., J.V., and S.A. carried out analysis and interpretation of data. J.V. and S.A. drafted the manuscript. All authors read and approved the final manuscript.

REFERENCES

1. Djoko KY, Ong CL, Walker MJ, McEwan AG. 2015. The role of copper and zinc toxicity in innate immune defense against bacterial pathogens. J Biol Chem 290:18954–18961. https://doi.org/10.1074/jbc.R115.647099.
2. Neyrolles O, Wolschendorf F, Mitra A, Niederweis M. 2015. Mycobacteria, metals, and the macrophage. Immunol Rev 264:249–263. https://doi.org/10.1111/imr.12265.
3. Stafford SL, Bokil NJ, Achard ME, Kapetanovic R, Schembri MA, McEwan AG, Sweet MJ. 2013. Metal ions in macrophage antimicrobial pathways: emerging roles for zinc and copper. Biosci Rep 33:e00049. https://doi.org/10.1042/BSR20130014.
4. Hood MI, Skaar EP. 2012. Nutritional immunity: transition metals at the pathogen-host interface. Nat Rev Microbiol 10:525–537. https://doi.org/10.1038/nrmicro2836.
5. Flo TH, Smith KD, Sato S, Rodriguez DJ, Holmes MA, Strong RK, Akira S, Aderem A. 2004. Lipocalin 2 mediates an innate immune response to bacterial infection by sequestrating iron. Nature 432:917–921. https://doi.org/10.1038/nature03104.
6. Kehl-Fie TE, Skaar EP. 2010. Nutritional immunity beyond iron: a role for manganese and zinc. Curr Opin Chem Biol 14:218–224. https://doi.org/10.1016/j.cbpa.2009.11.008.
7. Cellier MF, Courville P, Campion C. 2007. Nramp1 phagocyte intracellular metal withdrawal defense. Microbes Infect 9:1662–1670. https://doi.org/10.1016/j.micinf.2007.09.006.
8. Juttukonda LJ, Skaar EP. 2015. Manganese homeostasis and utilization in pathogenic bacteria. Mol Microbiol 97:216–228. https://doi.org/10.1111/mmi.13034.
9. Lisher JP, Giedroc DP. 2013. Manganese acquisition and homeostasis at the host-pathogen interface. Front Cell Infect Microbiol 3:91. https://doi.org/10.3389/fcimb.2013.00091.
10. Aguirre JD, Culotta VC. 2012. Battles with iron: manganese in oxidative stress protection. J Biol Chem 287:13541–13548. https://doi.org/10.1074/jbc.R111.312181.
11. Anjem A, Varghese S, Imlay JA. 2009. Manganese import is a key element of the OxyR response to hydrogen peroxide in Escherichia coli. Mol Microbiol 72:844–858. https://doi.org/10.1111/j.1365-2958.2009.06699.x.
12. Gaballa A, Wang T, Ye RW, Helmann JD. 2002. Functional analysis of the

Bacillus subtilis Zur regulon. J Bacteriol 184:6508–6514. https://doi.org/10.1128/jb.184.23.6508-6514.2002.
13. Oteiza PI. 2012. Zinc and the modulation of redox homeostasis. Free Radic Biol Med 53:1748–1759. https://doi.org/10.1016/j.freeradbiomed.2012.08.568.
14. Janulczyk R, Ricci S, Bjorck L. 2003. MtsABC is important for manganese and iron transport, oxidative stress resistance, and virulence of Streptococcus pyogenes. Infect Immun 71:2656–2664. https://doi.org/10.1128/iai.71.5.2656-2664.2003.
15. Turner AG, Ong C-LY, Gillen CM, Davies MR, West NP, McEwan AG, Walker MJ. 2015. Manganese homeostasis in group A Streptococcus is critical for resistance to oxidative stress and virulence. mBio 6:e00278-15. https://doi.org/10.1128/mBio.00278-15.
16. Chandrangsu P, Rensing C, Helmann JD. 2017. Metal homeostasis and resistance in bacteria. Nat Rev Microbiol 15:338–350. https://doi.org/10.1038/nrmicro.2017.15.
17. Glasfeld A, Guedon E, Helmann JD, Brennan RG. 2003. Structure of the manganese-bound manganese transport regulator of Bacillus subtilis. Nat Struct Biol 10:652–657. https://doi.org/10.1038/nsb951.
18. Que Q, Helmann JD. 2000. Manganese homeostasis in Bacillus subtilis is regulated by MntR, a bifunctional regulator related to the diphtheria toxin repressor family of proteins. Mol Microbiol 35:1454–1468. https://doi.org/10.1046/j.1365-2958.2000.01811.x.
19. Guedon E, Moore CM, Que Q, Wang T, Ye RW, Helmann JD. 2003. The global transcriptional response of Bacillus subtilis to manganese involves the MntR, Fur, TnrA and sigmaB regulons. Mol Microbiol 49:1477–1491. https://doi.org/10.1046/j.1365-2958.2003.03648.x.
20. Helmann JD. 2014. Specificity of metal sensing: iron and manganese homeostasis in Bacillus subtilis. J Biol Chem 289:28112–28120. https://doi.org/10.1074/jbc.R114.587071.
21. Huang X, Shin JH, Pinochet-Barros A, Su TT, Helmann JD. 2017. Bacillus subtilis MntR coordinates the transcriptional regulation of manganese uptake and efflux systems. Mol Microbiol 103:253–268. https://doi.org/10.1111/mmi.13554.
22. Moore CM, Helmann JD. 2005. Metal ion homeostasis in Bacillus subtilis. Curr Opin Microbiol 8:188–195. https://doi.org/10.1016/j.mib.2005.02.007.
23. Gaballa A, Helmann JD. 1998. Identification of a zinc-specific metalloregulatory protein, Zur, controlling zinc transport operons in *Bacillus subtilis*. J Bacteriol 180:5815–5821.
24. Lee JW, Helmann JD. 2007. Functional specialization within the Fur family of metalloregulators. Biometals 20:485–499. https://doi.org/10.1007/s10534-006-9070-7.
25. Outten CE, Tobin DA, Penner-Hahn JE, O'Halloran TV. 2001. Characterization of the metal receptor sites in *Escherichia coli* Zur, an ultrasensitive zinc(II) metalloregulatory protein. Biochemistry 40:10417–10423. https://doi.org/10.1021/bi0155448.
26. Patzer SI, Hantke K. 1998. The ZnuABC high-affinity zinc uptake system and its regulator Zur in *Escherichia coli*. Mol Microbiol 28:1199–1210. https://doi.org/10.1046/j.1365-2958.1998.00883.x.
27. Akanuma G, Nanamiya H, Natori Y, Nomura N, Kawamura F. 2006. Liberation of zinc-containing L31 (RpmE) from ribosomes by its paralogous gene product, YtiA, in *Bacillus subtilis*. J Bacteriol 188:2715–2720. https://doi.org/10.1128/JB.188.7.2715-2720.2006.
28. Gabriel SE, Helmann JD. 2009. Contributions of Zur-controlled ribosomal proteins to growth under zinc starvation conditions. J Bacteriol 191:6116–6122. https://doi.org/10.1128/JB.00802-09.
29. Nanamiya H, Kawamura F. 2010. Towards an elucidation of the roles of the ribosome during different growth phases in *Bacillus subtilis*. Biosci Biotechnol Biochem 74:451–461. https://doi.org/10.1271/bbb.90859.
30. Natori Y, Nanamiya H, Akanuma G, Kosono S, Kudo T, Ochi K, Kawamura F. 2007. A fail-safe system for the ribosome under zinc-limiting conditions in Bacillus subtilis. Mol Microbiol 63:294–307. https://doi.org/10.1111/j.1365-2958.2006.05513.x.
31. Prestel E, Noirot P, Auger S. 2015. Genome-wide identification of Bacillus subtilis Zur-binding sites associated with a Zur box expands its known regulatory network. BMC Microbiol 15:13. https://doi.org/10.1186/s12866-015-0345-4.
32. Ma Z, Gabriel SE, Helmann JD. 2011. Sequential binding and sensing of Zn(II) by *Bacillus subtilis* Zur. Nucleic Acids Res 39:9130–9138. https://doi.org/10.1093/nar/gkr625.
33. Ma Z, Helmann JD. 2013. Metal homeostasis and oxidative stress in *Bacillus subtilis*, eibc2129. In Scott RA (ed), Encyclopedia of inorganic and bioinorganic chemistry. John Wiley & Sons, Chichester, UK.
34. Chandrangsu P, Huang X, Gaballa A, Helmann JD. 2019. Bacillus subtilis FolE is sustained by the ZagA zinc metallochaperone and the alarmone ZTP under conditions of zinc deficiency. Mol Microbiol 112:751. https://doi.org/10.1111/mmi.14314.
35. Baichoo N, Wang T, Ye R, Helmann JD. 2002. Global analysis of the Bacillus subtilis Fur regulon and the iron starvation stimulon. Mol Microbiol 45:1613–1629. https://doi.org/10.1046/j.1365-2958.2002.03113.x.
36. Kleijn RJ, Buescher JM, Le Chat L, Jules M, Aymerich S, Sauer U. 2010. Metabolic fluxes during strong carbon catabolite repression by malate in Bacillus subtilis. J Biol Chem 285:1587–1596. https://doi.org/10.1074/jbc.M109.061747.
37. Lerondel G, Doan T, Zamboni N, Sauer U, Aymerich S. 2006. YtsJ has the major physiological role of the four paralogous malic enzyme isoforms in Bacillus subtilis. J Bacteriol 188:4727–4736. https://doi.org/10.1128/JB.00167-06.
38. Sauer U, Hatzimanikatis V, Bailey JE, Hochuli M, Szyperski T, Wuthrich K. 1997. Metabolic fluxes in riboflavin-producing Bacillus subtilis. Nat Biotechnol 15:448–452. https://doi.org/10.1038/nbt0597-448.
39. Schilling O, Frick O, Herzberg C, Ehrenreich A, Heinzle E, Wittmann C, Stulke J. 2007. Transcriptional and metabolic responses of Bacillus subtilis to the availability of organic acids: transcription regulation is important but not sufficient to account for metabolic adaptation. Appl Environ Microbiol 73:499–507. https://doi.org/10.1128/AEM.02084-06.
40. Agledal L, Niere M, Ziegler M. 2010. The phosphate makes a difference: cellular functions of NADP. Redox Rep 15:2–10. https://doi.org/10.1179/174329210X12650506623122.
41. Gaballa A, Chi BK, Roberts AA, Becher D, Hamilton CJ, Antelmann H, Helmann JD. 2014. Redox regulation in Bacillus subtilis: the bacilliredoxins BrxA(YphP) and BrxB(YqiW) function in de-bacillithiolation of S-bacillithiolated OhrR and MetE. Antioxid Redox Signal 21:357–367. https://doi.org/10.1089/ars.2013.5327.
42. Hoper D, Volker U, Hecker M. 2005. Comprehensive characterization of the contribution of individual SigB-dependent general stress genes to stress resistance of Bacillus subtilis. J Bacteriol 187:2810–2826. https://doi.org/10.1128/JB.187.8.2810-2826.2005.
43. Mascher T, Zimmer SL, Smith TA, Helmann JD. 2004. Antibiotic-inducible promoter regulated by the cell envelope stress-sensing two-component system LiaRS of Bacillus subtilis. Antimicrob Agents Chemother 48:2888–2896. https://doi.org/10.1128/AAC.48.8.2888-2896.2004.
44. Seydlová G, Halada P, Fišer R, Toman O, Ulrych A, Svobodová J. 2012. DnaK and GroEL chaperones are recruited to the Bacillus subtilis membrane after short-term ethanol stress. J Appl Microbiol 112:765–774. https://doi.org/10.1111/j.1365-2672.2012.05238.x.
45. Susin MF, Baldini RL, Gueiros-Filho F, Gomes SL. 2006. GroES/GroEL and DnaK/DnaJ have distinct roles in stress responses and during cell cycle progression in Caulobacter crescentus. J Bacteriol 188:8044–8053. https://doi.org/10.1128/JB.00824-06.
46. Sugimoto S, Higashi C, Matsumoto S, Sonomoto K. 2010. Improvement of multiple-stress tolerance and lactic acid production in Lactococcus lactis NZ9000 under conditions of thermal stress by heterologous expression of Escherichia coli dnaK. Appl Environ Microbiol 76:4277–4285. https://doi.org/10.1128/AEM.02878-09.
47. Koskiniemi S, Lamoureux JG, Nikolakakis KC, t'Kint de Roodenbeke C, Kaplan MD, Low DA, Hayes CS. 2013. Rhs proteins from diverse bacteria mediate intercellular competition. Proc Natl Acad Sci U S A 110:7032–7037. https://doi.org/10.1073/pnas.1300627110.
48. Haider S, Pal R. 2013. Integrated analysis of transcriptomic and proteomic data. Curr Genomics 14:91–110. https://doi.org/10.2174/1389202911314020003.
49. Chillappagari S, Miethke M, Trip H, Kuipers OP, Marahiel MA. 2009. Copper acquisition is mediated by YcnJ and regulated by YcnK and CsoR in Bacillus subtilis. J Bacteriol 191:2362–2370. https://doi.org/10.1128/JB.01616-08.
50. Solovieva IM, Entian KD. 2002. Investigation of the yvgW Bacillus subtilis chromosomal gene involved in Cd(2+) ion resistance. FEMS Microbiol Lett 208:105–109. https://doi.org/10.1111/j.1574-6968.2002.tb11068.x.
51. Carballido-López R. 2019. Rod width under control. Nat Microbiol 4:1246. https://doi.org/10.1038/s41564-019-0528-0.
52. Dajkovic A, Tesson B, Chauhan S, Courtin P, Keary R, Flores P, Marliere C, Filipe SR, Chapot-Chartier MP, Carballido-Lopez R. 2017. Hydrolysis of peptidoglycan is modulated by amidation of meso-diaminopimelic acid and M g2+ in B acillus subtilis. Mol Microbiol 104:972–988. https://doi.org/10.1111/mmi.13673.
53. Arakha M, Saleem M, Mallick BC, Jha S. 2015. The effects of interfacial

potential on antimicrobial propensity of ZnO nanoparticle. Sci Rep 5:9578. https://doi.org/10.1038/srep09578.
54. Solopova A, Formosa-Dague C, Courtin P, Furlan S, Veiga P, Péchoux C, Armalyte J, Sadauskas M, Kok J, Hols P, Dufrêne YF, Kuipers OP, Chapot-Chartier M-P, Kulakauskas S. 2016. Regulation of cell wall plasticity by nucleotide metabolism in Lactococcus lactis. J Biol Chem 291: 11323–11336. https://doi.org/10.1074/jbc.M116.714303.
55. Halder S, Yadav KK, Sarkar R, Mukherjee S, Saha P, Haldar S, Karmakar S, Sen T. 2015. Alteration of Zeta potential and membrane permeability in bacteria: a study with cationic agents. SpringerPlus 4:672. https://doi.org/10.1186/s40064-015-1476-7.
56. Tavares AFN, Teixeira M, Romão CC, Seixas JD, Nobre LS, Saraiva LM. 2011. Reactive oxygen species mediate bactericidal killing elicited by carbon monoxide-releasing molecules. J Biol Chem 286:26708–26717. https://doi.org/10.1074/jbc.M111.255752.
57. Chen L, James LP, Helmann JD. 1993. Metalloregulation in Bacillus subtilis: isolation and characterization of two genes differentially repressed by metal ions. J Bacteriol 175:5428–5437. https://doi.org/10.1128/jb.175.17.5428-5437.1993.
58. Fuangthong M, Herbig AF, Bsat N, Helmann JD. 2002. Regulation of the Bacillus subtilis fur and perR genes by PerR: not all members of the PerR regulon are peroxide inducible. J Bacteriol 184:3276–3286. https://doi.org/10.1128/jb.184.12.3276-3286.2002.
59. Gaballa A, Helmann JD. 2002. A peroxide-induced zinc uptake system plays an important role in protection against oxidative stress in Bacillus subtilis. Mol Microbiol 45:997–1005. https://doi.org/10.1046/j.1365-2958.2002.03068.x.
60. Herbig AF, Helmann JD. 2001. Roles of metal ions and hydrogen peroxide in modulating the interaction of the Bacillus subtilis PerR peroxide regulon repressor with operator DNA. Mol Microbiol 41:849–859. https://doi.org/10.1046/j.1365-2958.2001.02543.x.
61. Smith KF, Bibb LA, Schmitt MP, Oram DM. 2009. Regulation and activity of a zinc uptake regulator, Zur, in Corynebacterium diphtheriae. J Bacteriol 191:1595–1603. https://doi.org/10.1128/JB.01392-08.
62. Fischer E, Sauer U. 2005. Large-scale in vivo flux analysis shows rigidity and suboptimal performance of Bacillus subtilis metabolism. Nat Genet 37:636–640. https://doi.org/10.1038/ng1555.
63. Luche S, Eymard-Vernain E, Diemer H, Van Dorsselaer A, Rabilloud T, Lelong C. 2016. Zinc oxide induces the stringent response and major reorientations in the central metabolism of Bacillus subtilis. J Proteomics 135:170–180. https://doi.org/10.1016/j.jprot.2015.07.018.
64. Ong CL, Walker MJ, McEwan AG. 2015. Zinc disrupts central carbon metabolism and capsule biosynthesis in Streptococcus pyogenes. Sci Rep 5:10799. https://doi.org/10.1038/srep10799.
65. Smaldone GT, Revelles O, Gaballa A, Sauer U, Antelmann H, Helmann JD. 2012. A global investigation of the Bacillus subtilis iron-sparing response identifies major changes in metabolism. J Bacteriol 194:2594–2605. https://doi.org/10.1128/JB.05990-11.
66. Wilks JC, Kitko RD, Cleeton SH, Lee GE, Ugwu CS, Jones BD, BonDurant SS, Slonczewski JL. 2009. Acid and base stress and transcriptomic responses in Bacillus subtilis. Appl Environ Microbiol 75:981–990. https://doi.org/10.1128/AEM.01652-08.
67. Inaoka T, Matsumura Y, Tsuchido T. 1999. SodA and manganese are essential for resistance to oxidative stress in growing and sporulating cells of Bacillus subtilis. J Bacteriol 181:1939–1943.
68. Dwyer DJ, Kohanski MA, Collins JJ. 2009. Role of reactive oxygen species in antibiotic action and resistance. Curr Opin Microbiol 12:482–489. https://doi.org/10.1016/j.mib.2009.06.018.
69. Ming LJ. 2003. Structure and function of "metalloantibiotics". Med Res Rev 23:697–762. https://doi.org/10.1002/med.10052.
70. Zarkan A, Macklyne HR, Chirgadze DY, Bond AD, Hesketh AR, Hong HJ. 2017. Zn(II) mediates vancomycin polymerization and potentiates its antibiotic activity against resistant bacteria. Sci Rep 7:4893. https://doi.org/10.1038/s41598-017-04868-2.
71. Auger S, Henry C, Pechoux C, Suman S, Lejal N, Bertho N, Larcher T, Stankic S, Vidic J. 2018. Exploring multiple effects of Zn0.15Mg0.85O nanoparticles on Bacillus subtilis and macrophages. Sci Rep 8:12276. https://doi.org/10.1038/s41598-018-30719-9.
72. Harwood CR, Cutting SM (ed). 1990. Molecular biological methods for Bacillus. Wiley, Chichester, United Kingdom.
73. Kunst F, Rapoport G. 1995. Salt stress is an environmental signal affecting degradative enzyme synthesis in Bacillus subtilis. J Bacteriol 177: 2403–2407. https://doi.org/10.1128/jb.177.9.2403-2407.1995.
74. He X, Liu B. 2017. Oolong tea extract as a substitute for uranyl acetate in staining of ultrathin sections based on examples of animal tissues for transmission electron microscopy. J Microsc 267:27–33. https://doi.org/10.1111/jmi.12544.
75. Randazzo P, Aubert-Frambourg A, Guillot A, Auger S. 2016. The MarR-like protein PchR (YvmB) regulates expression of genes involved in pulcherriminic acid biosynthesis and in the initiation of sporulation in Bacillus subtilis. BMC Microbiol 16:190. https://doi.org/10.1186/s12866-016-0807-3.
76. Nicolas P, Mäder U, Dervyn E, Rochat T, Leduc A, Pigeonneau N, Bidnenko E, Marchadier E, Hoebeke M, Aymerich S, Becher D, Bisicchia P, Botella E, Delumeau O, Doherty G, Denham EL, Fogg MJ, Fromion V, Goelzer A, Hansen A, Härtig E, Harwood CR, Homuth G, Jarmer H, Jules M, Klipp E, Le Chat L, Lecointe F, Lewis P, Liebermeister W, March A, Mars RAT, Nannapaneni P, Noone D, Pohl S, Rinn B, Rügheimer F, Sappa PK, Samson F, Schaffer M, Schwikowski B, Steil L, Stülke J, Wiegert T, Devine KM, Wilkinson AJ, van Dijl JM, Hecker M, Völker U, Bessières P, Noirot P. 2012. Condition-dependent transcriptome reveals high-level regulatory architecture in *Bacillus subtilis*. Science 335:1103–1106. https://doi.org/10.1126/science.1206848.
77. Michna RH, Commichau FM, Tödter D, Zschiedrich CP, Stülke J. 2014. Subti wiki—a database for the model organism Bacillus subtilis that links pathway, interaction and expression information. Nucleic Acids Res 42:D692–D698. https://doi.org/10.1093/nar/gkt1002.